PCCP

ROYAL SOCIETY OF CHEMISTRY

PAPER

View Article Online
View Journal | View Issue

Cite this: *Phys. Chem. Chem. Phys.*, 2025, **27**, 9631

Thermal degradation energetics of fentanyl and its analogues: furanyl fentanyl and *ortho*-fluoro fentanyl†

Bharat Poudel,[a] Joshua J. Whiting,[b] Juan M. Vanegas*[c] and Susan B. Rempe*[d]

Fentanyl is a synthetic opioid with higher potency compared to morphine and heroin, making it an essential drug for pain management and also an abused drug. Beyond fentanyl, derivatives, such as *o*-fluoro fentanyl and furanyl fentanyl, also possess similar potency and present a significant risk of misuse, but without medical utility. A major challenge for law enforcement is detecting fentanyl and its analogues in their degraded forms. While the degradation fragments of fentanyl are well-known, those of its analogues are not as well studied. Here, we investigated the thermal degradation pathways of fentanyl analogues using extensive *ab initio* molecular dynamics simulations combined with enhanced sampling techniques, including multiple walker metadynamics and umbrella sampling. We calculated the free energy profiles for each bond previously identified as a potential degradation site to map out the thermodynamic driving forces. Additionally, we estimated the forward attempt rate of each bond degradation reaction to gain insights into the kinetics of those degradation processes. Our results show that, despite high similarity in structure, the bond breaking pathways differ for the analogues compared with fentanyl. We also observed that traditional force fields with fixed charges are insufficient for studies of fentanyl and its analogues due to polarizability of the electronic structure. Distribution Statement A. Approved for Public Release. Distribution Unlimited.

Received 2nd January 2025,
Accepted 9th April 2025

DOI: 10.1039/d5cp00024f

rsc.li/pccp

1. Introduction

Fentanyl is a synthetic opioid used to manage pain due to its order-of-magnitude higher potency than both morphine and heroin. Fentanyl is also well-known as an abused drug with lethal outcomes.[1,2] Efforts to detect illicit fentanyl focus on its thermal degradation reactions, and the products of those reactions are well-known.[3–5] Less known are the fentanyl analogues, such as furanyl and *o*-fluoro fentanyl. Despite having comparable potency and similar structure to fentanyl (Fig. 1), they have not been useful medically.[6] Synthesized in part to evade detection in standard drug tests, the analogues are also lethal. In a recent study of compounds found in unintentional drug overdoses in Ohio, about one-third of the cases involved furanyl fentanyl.[7] Similarly, *o*-fluoro fentanyl is also known for illegal use, eventually causing death.

The current detection devices are designed to identify fentanyl and its analogues in their undegraded forms. However, these opioids can degrade when exposed to high temperature, making it even more challenging to detect them through their

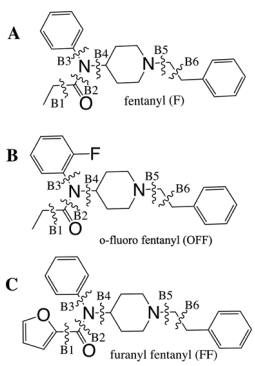

Fig. 1 Chemical structures along with the bonds of interest are shown for (A) fentanyl, and its analogues, (B) *o*-fluoro fentanyl (OFF), and (C) furanyl fentanyl (FF).

[a] *Environmental Systems Biology, Sandia National Laboratories, Albuquerque, NM, USA*
[b] *Biological and Chemical Sensors, Sandia National Laboratories, Albuquerque, NM, USA*
[c] *Department of Biochemistry and Biophysics, Oregon State University, Corvallis, OR, USA. E-mail: vanegasj@oregonstate.edu*
[d] *Center for Integrated Nanotechnologies, Sandia National Laboratories, Albuquerque, NM, USA. E-mail: slrempe@sandia.gov*

† Electronic supplementary information (ESI) available. See DOI: https://doi.org/10.1039/d5cp00024f

degradation products, especially if those degradants are unknown. Different methods exist to degrade fentanyl, including thermal[3–5] and oxidative degradation,[8] and acid and base treatment.[9] The most effective and studied means of degradation is thermal degradation.

The degradation of fentanyl and its analogues can yield other toxic compounds with the potential of being abused.[5] For example, norfentanyl[5,10] and furanyl norfentanyl form after the degradation of fentanyl and furanyl fentanyl, respectively. Unintentional overdose of these analogues also causes deaths.[7] Despite the ongoing opioid epidemic in Western countries due to fentanyl and its analogs, no thermal degradation studies have been done for *o*-fluoro fentanyl and furanyl fentanyl. Here, we focus on the thermal degradation reactions of furanyl and *o*-fluoro fentanyl, and compare with fentanyl, to aide in the detection of these fentanyl analogues.[11,12]

In terms of chemical structure, there are notable differences between fentanyl, *o*-fluoro fentanyl, and furanyl fentanyl. While they share the same *N*-alkyl chain and piperidine ring, they differ in the aniline ring and amide groups. Studies have shown that nuanced structural differences result in the different efficacy and potency of the fentanyl analogues.[13] The main degradation site for bond breaking in fentanyl occurs near the nitrogen atoms that are in close proximity with the aniline ring, amide group and piperidine ring.[3–5,14]

All studies to date, per our knowledge, have reported on the primary and secondary mechanisms of fentanyl degradation.[3–5,15] However, the degradation mechanism for furanyl fentanyl and *o*-fluoro fentanyl, specifically the bond-breaking processes and their energetics, along with the possible fragments after degradation, have received little attention. In this study, we investigate the possible degradants of those fentanyl analogues by computing the free energies associated with bond breaking through extensive *ab initio* molecular dynamics (AIMD) simulations combined with the well-tempered multiple-walker metadynamics approach, and study the electron density of the different analogues.

2. Materials and methods

2.1. AIMD simulations and free energy calculations

AIMD simulations were conducted using the Quickstep[16] module of the CP2K software package,[17] which facilitates density functional theory (DFT) calculations through the Gaussian and plane waves method (GPW). We use DFT without incorporating dispersion corrections in our study. Previous research has indicated that dispersion-corrected DFT does not exhibit better performance in ionic systems[18] although it has demonstrated improved accuracy in other types of systems.[19–23] While our results may have limitations due to the absence of dispersion corrections, the calculation of activation energies ($\Delta F^{\dagger}$), determined as the difference between two extrema, effectively mitigates the potential errors.

The LSD (local spin density) approximation was used in all AIMD simulations to enable spin-unrestricted Kohn–Sham solutions. The PBE (Perdew–Burke–Ernzerhof) generalized gradient approximation[24] was used for the exchange–correlation functional in the electronic structure DFT calculations. Wave function optimization at each self-consistent field (SCF) step was performed with the orbital transformation method[25] and direct inversion in the iterative subspace method, also known as Pulay mixing. The optimized double-zeta basis set (DZVP-MOLOPT) was applied to all the atoms together with the Goedecker–Teter–Hutter (GTH) pseudopotentials.[26–29] The geometry optimization was performed using a conjugate gradient algorithm before running the MD simulation. A time step of 0.5 femtoseconds (fs) was selected for the dynamics, and a Nose–Hoover thermostat was used to maintain a constant temperature of 1273 K. This elevated temperature, compared to experimental conditions, was chosen to expedite the dynamics due to the limited simulation timescale, which was within the picosecond range. All simulations were performed within a fixed rectangular cell of dimensions 0.3 nm × 0.3 nm × 0.3 nm.

The electrostatic potential (ESP) of the atomic partial charges was determined using the Breneman model, which is known for accurately reproducing the molecular electrostatic potential. This model is implemented in Q-Chem as the ChElPG (charge extrapolation using the Lagrange points grid) method to compute partial charges.[30] Initially, the structure was optimized with the VDZ (valence-double-zeta) basis set using the PBE generalized gradient approximation for the exchange–correlation functional in the DFT calculations, followed by a single-point calculation. The choice of basis set and functional are explained in the (ESI†), Fig. S3.

Free energy calculations were performed with CP2K together with the PLUMED plugin.[31,32] The free energy computed here is a potential of mean force (PMF) and corresponds to the Helmholtz free energy as it is computed under constant temperature, but not constant pressure. The activation energy is determined by calculating the difference in free energy at the position of the maximum and the position of the minimum. Equilibrium geometries correspond to the minima of the PMFs along the various reaction coordinates, determined by optimization of the energy and confirmed by normal mode analysis and the absence of negative frequencies.[33] The position of the maximum corresponds to a transition state along the chosen bond breaking coordinate.

To compute the activation free energy of bond breaking at selected bonds, steered molecular dynamics (MD) simulations were first employed, with bond length (d) as the collective variable (CV), also known as a reaction coordinate. A spring constant of 1 000 000 kJ mol^{-1} nm^{-2} was used for the time-dependent harmonic restraint potential that linearly increases the bond length up to ~0.6 nm. Following the steered CV simulation, 10 configurations were chosen at regular intervals along the bond CV and equilibrated for 0.5 ps while holding each bond length fixed with a fixed harmonic potential. We used these 10 configurations to run multiple-walker well-tempered metadynamics to compute the free energy along the chosen reaction coordinates.[34,35] Again, the difference in free energy from the position of the maximum to the position of the minimum defines the activation energy, $\Delta F^{\dagger}$.

In the metadynamics runs, the simulations were biased with a time-dependent (t) potential (V) of the form,

$$V(d,t) = \sum_{t'}^{t' < t} W \exp\left(-\frac{V(\mathrm{d}(t'),\, t')}{k_{\mathrm{B}}\Delta T}\right) \exp\left(-\frac{(\mathrm{d} - \mathrm{d}(t'))^2}{2\sigma^2}\right), \quad (1)$$

where W and σ are the height and width of the added Gaussian hills. ΔT is a fictitious maximum increase in temperature that ensures convergence by limiting the extent of the free energy exploration, and k_{B} is Boltzmann's constant. At long timescales, the unbiased free energy, $F(d)$, can be recovered from

$$V(d,\, t \to \infty) = -\frac{\Delta T}{T + \Delta T} F(d) + C, \quad (2)$$

where C is an immaterial constant. The value of ΔT is set by the 'bias factor' parameter, $b = \frac{T + \Delta T}{T}$, and the frequency of addition of Gaussian hills is determined by a fixed deposition rate, ω. The same values of σ = 0.01 nm, b = 15, W = 5.3 kJ mol^{-1}, and ω = 30 fs were used for all free energy calculations. The value of σ was chosen based on the standard deviation of the bond lengths observed during equilibrium simulations. Similarly, the value of ω was chosen to be greater than the typical period of oscillation of the bond lengths. The initial value of the hill height was chosen to be $\frac{k_{\mathrm{B}}T}{2} = \frac{10.58\ \mathrm{kJ\ mol^{-1}}}{2}$, where, k_{B} is the Boltzmann constant. The bias factor value of b = 15 was chosen so that a barrier on the order of 200 kJ mol^{-1} would be within reach of any given walker $\left(b < \frac{200\ \mathrm{kJ\ mol^{-1}}}{10.58\ \mathrm{kJ\ mol^{-1}}} = 19\right)$. All walkers were then simultaneously run in simulation time spans from 17.20 to 23.82 ps each using well-tempered metadynamics. Therefore, the combined simulation time used to obtain each free energy surface was $>>$ 170 ps.

All the simulation settings are similar to our previously published work on fentanyl to enable direct comparison with the current results of fentanyl analogues.[14] While other approaches to computing free energy profiles are available, including umbrella sampling,[36] the metadynamics method has the advantage of not requiring prior knowledge of free energy barriers. This freedom has proven advantageous in studies of transport[37] and receptor proteins,[38] in addition to the current systems. Convergence of the free energy profiles along the reaction coordinates was monitored by computing the difference between the minimum (F_{min}, at the equilibrium bond length) and the maximum (F_{max}, at the transition barrier) free energy values in 2 ps intervals (per walker). The Python Matplotlib library was used to generate the plots.[39]

3. Results and discussion

3.1. Thermal degradation pathways of fentanyl analogues

We explored the degradation pathways of furanyl fentanyl and *o*-fluoro fentanyl by characterizing the free energy required for breaking specific bonds of interest. The free energy was computed in the gas phase because of its relevance to drug detection. We computed the activation free energy of bond breaking in *ab initio* molecular dynamics (AIMD) simulations by stretching a particular bond using a steered harmonic potential until the atoms were no longer bonded, followed by a well-tempered metadynamics simulation (see Materials and methods section).

We chose six different bonds of interest, matching those reported on earlier for fentanyl.[14] Experimental studies showed those bonds are the possible specific sites for bond breaking in fentanyl. Previous experimental pyrolytic studies[3–5] determined that fragmentation is most likely at the N–C bonds, particularly near the piperidine ring. The furanyl fentanyl and *o*-fluoro fentanyl also share the same piperidine ring with fentanyl.

We estimated the free energy of bond breaking between the bonds made by the N and C atoms (Fig. 2) starting with the cleavage of bond B4 in both analogs, a process that earlier produced the PEP (phenylethyl piperidine) and PRP (propionanilide) fragments in fentanyl.[14] Those fragments were also identified experimentally following thermal degradation of fentanyl. The computed free energy values for the breaking of bond B4 in *o*-fluoro fentanyl and furanyl fentanyl at a temperature of 1273 K were determined to be 130 and 85 kJ mol^{-1}, respectively (Fig. 2C). A comparative analysis, represented by the black dashed plot for bond breaking in fentanyl (105 kJ mol^{-1}), reveals that the likelihood of bond B4 breaking is greater for furanyl fentanyl than for fentanyl, while it is comparatively lower for *o*-fluoro fentanyl.

Further expansion of our interest to other bonds shows that the free energy evaluation for the breaking of bonds B2 (Fig. 2A), B3 (Fig. 2B), and B5 (Fig. 2D) in both analogues, furanyl fentanyl and *o*-fluoro fentanyl, demonstrate consistently higher values than those observed for fentanyl. The perspective from the activation free energies for all bonds within furanyl fentanyl indicates lower magnitudes in comparison to *o*-fluoro fentanyl. This trend suggests a propensity for weaker bonding relative to *o*-fluoro fentanyl across these specific bonds studied here.

In addition to our investigation of nitrogen-associated bonds, we conducted a systematic analysis of the free energy pertaining to carbon–carbon bonds within the analogues.

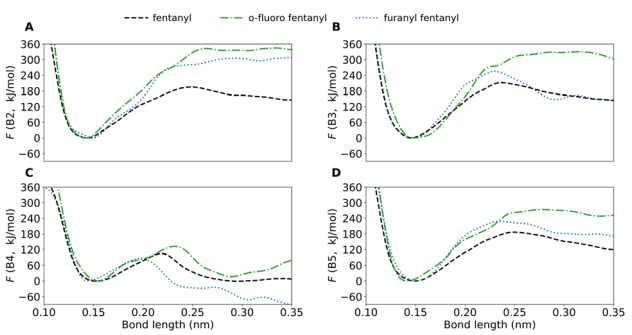

Fig. 2 The free energy profile of N–C bonds (A) B2, (B) B3, (C) B4, and (D) B5 for fentanyl (dashed black) and two analogues: furanyl fentanyl (blue) and *o*-fluoro fentanyl (green). Please refer to Fig. 1 for more information about the bonds.

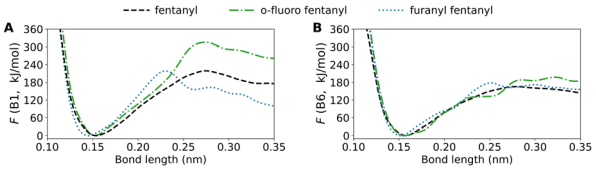

Fig. 3 The free energy profile of C–C bonds (A) B1, and (B) B6 for fentanyl (dashed black) and two analogues: furanyl fentanyl (blue), and *o*-fluoro fentanyl (green). Please refer to Fig. 1 for more information about the bonds.

The computed activation free energy for furanyl fentanyl concerning bond B1 (Fig. 3A) closely approximates that of fentanyl, measuring approximately 219 kJ mol^{-1}. However, a notable distinction is observed in *o*-fluoro fentanyl, where the corresponding activation free energy is significantly higher, at 316 kJ mol^{-1}.

Furthermore, the B6 bond (Fig. 3B), which yields toluene upon breaking, reveals higher bond-breaking activation free energy values for both *o*-fluoro fentanyl (197 kJ mol^{-1}) and furanyl fentanyl (178 kJ mol^{-1}) in contrast to fentanyl, recorded at 166 kJ mol^{-1}. Intriguingly, the observed variations in the activation free energy barriers of carbon–carbon bonds in furanyl and *o*-fluoro fentanyl do not exhibit a clear pattern in comparison to fentanyl. The convergence of free energy simulations for both furanyl fentanyl and *o*-fluoro fentanyl was monitored by the change in free energy as a function of time throughout the simulation period (shown in the ESI†).

3.1.1. Estimated forward kinetics from attempt rates. The detailed characterization of rare bond breaking events poses inherent challenges as those events are often elusive and computationally demanding. The computational expense associated with simulating transitions between reactant and product states further complicates the process. To overcome those challenges, we used a strategy to estimate the forward kinetics of bond breaking by leveraging the estimated activation free energy barrier and diffusive relaxation time as significant parameters. As a reminder, the activation energy is determined by calculating the difference in PMF along the reaction coordinate path (R) between its maximum and minimum values. While the free energy barrier obtained from our AIMD simulations may not be a true activation energy, as detailed by Johannes *et al.*,[40] it should still provide a reasonable estimate for the magnitude of the barrier. This approach allows for computation of a forward reaction attempt rate from the free energy barrier and the diffusive relaxation time.

We used an Arrhenius-Bell model to estimate the forward attempt rate, which refers to the probability of reactants crossing the free energy barrier.[41,42] The attempt rate can be estimated using

$$k_f = \frac{1}{t_D}\exp\left(\frac{-\Delta F^{\dagger}}{k_B T}\right), \quad (3)$$

where t_D is the diffusive relaxation time (inverse bond vibrational frequency). The diffusive relaxation is computed by quantifying the temporal variations in bond distances during the equilibrium (unbiased) simulations. We used Fourier analysis to extract the frequencies associated with those bond fluctuations.[33] $\Delta F^{\dagger}$ is the difference in free energy between reactants and the transition state, k_B is the Boltzmann constant and T is the temperature.

The forward attempt rate, k_f, depends on the spontaneous dissociation rate and on the difference in the free energy between the two states (reactant and transition states). Since k_f is exponentially related to the free energy difference, as shown in eqn (3), even a small change in free energy changes k_f significantly. We calculate the ratio of the forward attempt rate of all bonds to the forward attempt rate of B4 (k_f/k_f (B4)) to estimate the likelihood of bond breaking. The bond B4 of furanyl fentanyl is likely to break easily, followed by the same bond in fentanyl and *o*-fluoro fentanyl. The analysis results in finding that furanyl fentanyl has the highest forward reaction rate attempt ratio of 11 while fentanyl and *o*-fluoro fentanyl have ratios of 1 and 0.2 (see Table 1).

3.1.2. Effects on electron density due to structural changes. To gain insight about the differences in activation free energy and kinetics for bond breaking, we analyzed the charge distribution across four different structures: fentanyl, *o*-fluoro fentanyl, furanyl fentanyl, and an alternative structure of furanyl fentanyl where two oxygen atoms are oriented oppositely (Fig. 4). In *o*-fluoro fentanyl, the fluorine atom (F) withdraws negative charge (−0.22) from the carbon atoms of the phenyl group, resulting in the connected carbon atom having a positive charge of +0.35 (Fig. 4B). In contrast, the same carbon atom has a negative charge of −0.14 in the same position for fentanyl (Fig. 4A).

Similarly, we computed the partial charges for furanyl fentanyl in two different orientations: (a) with oxygen atoms facing the same direction, and (b) with oxygen atoms facing in opposite directions. Interestingly, these two orientations have different electron distributions. When two oxygen atoms face in the same direction, the aniline ring is more positive as compared when the oxygens face in opposite directions (Fig. 4C and D), resulting in different charges for the same atoms in each structure. This rotation of oxygen atoms increases the negative charge on the phenyl ring.

Table 1 Bond breaking dissociation time (t_D), free energy barrier ($\Delta F^{\dagger}$), and attempt rate (k_f). All the forward rates (k_f) are computed relative to B4 of fentanyl

Bonds	t_D (ps)	$\Delta F^{\dagger}$ (kJ mol^{-1})	k_f (s^{-1})	k_f/k_f (B4)
B1(F)	31.6	219 ± 2	3.1×10^{1}	2.2×10^{-5}
B1(OFF)	27.0	316 ± 2	4.0×10^{-3}	2.9×10^{-9}
B1(FF)	38.0	219 ± 5	2.7×10^{1}	2.0×10^{-5}
B2(F)	39.4	195 ± 3	2.6×10^{2}	1.8×10^{-4}
B2(OFF)	4.0	336 ± 2	4.0×10^{-3}	2.0×10^{-9}
B2(FF)	30.0	335 ± 7	6.0×10^{-4}	4.5×10^{-10}
B3(F)	49.7	212 ± 4	4.1×10^{1}	2.9×10^{-5}
B3(OFF)	12.0	230 ± 6	3.1×10^{1}	2.2×10^{-5}
B3(FF)	32.0	254 ± 2	1.2×10^{0}	8.4×10^{-5}
B4(F)	34.8	105 ± 2	1.4×10^{6}	1.0×10^{0}
B4(OFF)	16.0	130 ± 1	2.8×10^{5}	2.0×10^{-1}
B4(FF)	20.0	85 ± 2	1.6×10^{7}	1.1×10^{1}
B5(F)	30.7	186 ± 1	7.1×10^{2}	5.1×10^{-4}
B5(OFF)	33.0	273 ± 1	1.9×10^{-1}	1.2×10^{-7}
B5(FF)	34.0	228 ± 6	1.3×10^{1}	9.2×10^{-6}
B6(F)	34.1	166 ± 1	4.5×10^{3}	3.2×10^{-3}
B6(OFF)	7.0	197 ± 7	1.2×10^{3}	8.5×10^{-4}
B6(FF)	24.0	178 ± 7	2.1×10^{3}	1.9×10^{-3}

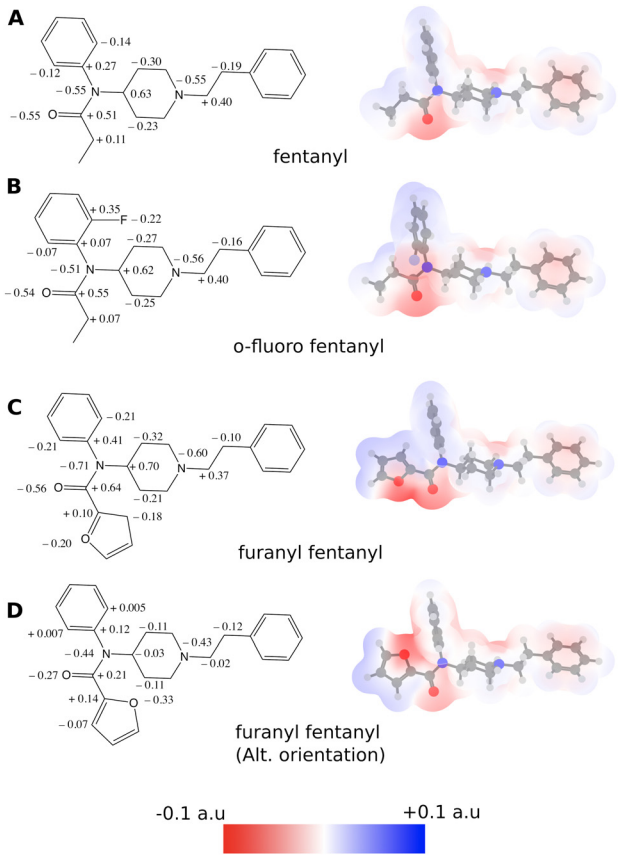

Fig. 4 Electron density of fentanyl and its analogues along with an alternate configuration of furanyl fentanyl. The partial charge of atoms (left) and corresponding electron density for (A) fentanyl, (B) *o*-fluoro fentanyl, and (C) furanyl fentanyl. In (D), the partial charge of furanyl fentanyl atoms in an alternative configuration (left) and the electron density (right).

4. Discussion

Our investigation involved extensive *ab initio* simulations with enhanced sampling techniques to compute the free energy barriers associated with bond breaking in furanyl fentanyl and *o*-fluoro fentanyl, and compared them with the analogous assessment for fentanyl. The theoretical outcomes for fentanyl bond breaking aligns with and also validates the experimental findings. A comparative analysis of the results for fentanyl and its analogues revealed that bonds associated with nitrogen, particularly bond B4, exhibit the highest propensity for bond breakage, with free energy barriers of 85 kJ mol^{-1}, 105 kJ mol^{-1}, and 130 kJ mol^{-1} for furanyl fentanyl, fentanyl, and *o*-fluoro fentanyl.

In further support of the free energy profiles, we computed the attempt rates, utilizing diffusive relaxation times and free energy barriers. The reference rate was established for bond B4 of fentanyl, with all other bond attempt rates calculated relative to it. The attempt rate for B4 of fentanyl was set to 1, while the corresponding rates for *o*-fluoro fentanyl and furanyl fentanyl were 0.20 and 11.4. This assessment of attempt rates is consistent with the trends observed in the free energy barriers, reinforcing the relative likelihoods of bond breaking in fentanyl and its analogues.

The electron density map helps explain why *o*-fluoro fentanyl has the highest bond breaking free energy barrier of the molecules considered here. In that case, the fluorine atom made the difference by altering the electron distribution of its phenyl ring. The study of the electron distribution of furanyl fentanyl at two different structures revealed that the electron cloud is affected by the orientation of the structure. This result emphasizes the need to revisit earlier studies that used fixed charge force fields.

5. Conclusion

The results derived from our *ab initio* simulations and electron distribution analysis suggest that the bond breaking patterns of fentanyl are matched in its analogues. The alignment of results between fentanyl and its analogues display robustness of the free energy analysis employed in identifying probable bond breaking motifs. Consequently, our approach expands the experimental observations and its applicability to predicting potential products of thermal degradation reactions, thereby providing valuable insights into bond breaking dynamics that may help detect analogues of fentanyl, in addition to fentanyl.

Conflicts of interest

The authors declare no competing financial interest.

Acknowledgements

The authors appreciate funding from the Department of Defense. This work was performed, in part, at the Center for Integrated Nanotechnologies, an Office of Science User Facility operated for the U.S. Department of Energy (DOE) Office of Science. Computations were performed, in part, on the Vermont Advanced Computing Core supported in part by NSF Award No. OAC-1827314. Sandia National Laboratories is a multimission laboratory managed and operated by National Technology & Engineering Solutions of Sandia, LLC (NTESS), a wholly owned subsidiary of Honeywell International Inc., for the U.S. Department of Energys National Nuclear Security Administration (DOE/NNSA) under the DE-NA0003525 contract. This written work is authored by an employee of NTESS. The employee, not NTESS, owns the right, title and interest in and to the written work and is responsible for its contents. Any subjective views or opinions that might be expressed in the written work do not necessarily represent the views of the US Government. The publisher acknowledges that the U.S. Government retains a non-exclusive, paid-up, irrevocable, world-wide license to publish or reproduce the published form of this written work or allow others to do so, for U.S. Government purposes. The DOE will provide public access to results of federally sponsored research in accordance with the DOE Public Access Plan. The authors declare no competing financial interest.

References

1 K. Hasegawa, K. Minakata, M. Suzuki and O. Suzuki, *Forensic Toxicol.*, 2022, **40**(2), 234–243.
2 D. E. A. US Department of Justice, *National Drug Threat Assessment*, 2024, **https://www.dea.gov/press-releases/2024/05/09/dea-releases-2024-national-drug-threat-assessment**.
3 R. K. Nishikawa, S. C. Bell, J. C. Kraner and P. S. Callery, *J. Anal. Toxicol.*, 2009, **33**, 418–422.
4 A. Garg, D. W. Solas, L. H. Takahashi and J. V. Cassella, *J. Pharm. Biomed. Anal.*, 2010, **53**, 325–334.
5 L. Manral, P. K. Gupta, M. V. S. Suryanarayana, K. Ganesan and R. C. Malhotra, *J. Therm. Anal. Calorim.*, 2009, **96**, 531–534.
6 D. M. Swanson, L. S. Hair, S. R. Strauch Rivers, B. C. Smyth, S. C. Brogan, A. D. Ventoso, S. L. Vaccaro and J. M. Pearson, *J. Anal. Toxicol.*, 2017, **41**, 498–502.
7 R. Daniulaityte, M. P. Juhascik, K. E. Strayer, I. E. Sizemore, K. E. Harshbarger, H. M. Antonides and R. R. Carlson, Overdose Deaths Related to Fentanyl and Its Analogs—Ohio, January-February 2017, 2017, **https://www.cdc.gov/mmwr/volumes/66/wr/mm6634a3.htm**.
8 L. Qi, Z. Cheng, G. Zuo, S. Li and Q. Fan, *Def. Sci. J.*, 2011, 30–35.
9 J. Lambrolous, G. A. Spanos, N. V. Lazaridis, T. S. Ingallinera and V. K. Rodriguez, *J. Pharm. Biomed. Anal.*, 1999, 705–716.
10 M. Bazley, M. Logan, C. Baxter, A. A. B. Robertson and J. T. Blanchfield, *Aust. J. Chem.*, 2020, 868–879.
11 A. Helland, W. R. Brede, L. S. Michelsen, P. O. M. Gundersen, H. Aarset, J. E. SkjølÅs and L. Slørdal, *J. Anal. Toxicol.*, 2017, **41**, 708–709.
12 Schedules of Controlled Substances: Temporary Placement of ortho-Fluorofentanyl, Tetrahydrofuranyl Fentanyl, and Methoxyacetyl Fentanyl Into Schedule I, 2017, **https://tinyurl.com/3aets3ps**.
13 N. B. Varshenya, S. H. Hassanien, M. C. Holt, D. L. Stevens, N. K. Layle, J. R. Bassman, D. M. Lula and P. M. Beardsley, *Pharmacol., Biochem. Behav.*, 2023, **226**, 173572.
14 B. Poudel, L. Monteith, J. P. Sammon, J. J. Whiting, M. W. Moorman, J. M. Vanegas and S. B. Rempe, *Phys. Chem. Chem. Phys.*, 2023, **25**, 30880–30886.
15 J. D. Rabinowitz, M. Wensley, P. Lloyd, D. Myers, W. Shen, A. Lu, C. Hodges, R. Hale, D. Mufson and A. Zaffaroni, *J. Pharmacol. Exp. Ther.*, 2004, **309**, 769–775.
16 J. VandeVondele, M. Krack, F. Mohamed, M. Parrinello, T. Chassaing and J. Hutter, *Comput. Phys. Commun.*, 2005, **167**, 103–128.
17 T. D. Kühne, *et al.*, *J. Chem. Phys.*, 2020, **152**, 194103.
18 M. Soniat, D. M. Rogers and S. B. Rempe, *J. Chem. Theory Comput.*, 2015, **11**, 2958–2967.
19 S. Grimme, S. Ehrlich and L. Goerigk, *J. Comput. Chem.*, 2011, **32**, 1456–1465.
20 S. Grimme and M. Steinmetz, *Phys. Chem. Chem. Phys.*, 2013, **15**, 16031–16042.
21 L. Goerigk, *J. Chem. Theory Comput.*, 2014, **10**, 968–980.
22 J. D. Chai and M. Head-Gordon, *Phys. Chem. Chem. Phys.*, 2008, **10**, 6615–6620.
23 U. R. Fogueri, K. A. Kozuch and J. M. L. Martin, *J. Phys. Chem. A*, 2013, **117**, 2269–2277.
24 J. Perdew, K. Burke and M. Ernzerhof, *Phys. Rev. Lett.*, 1996, **77**, 3865–3868.
25 J. VandeVondele and J. Hutter, *J. Chem. Phys.*, 2003, **118**, 4365–4369.
26 J. VandeVondele and J. Hutter, *J. Chem. Phys.*, 2007, **127**, 114105.
27 S. Goedecker, M. Teter and J. Hutter, *Phys. Rev. B: Condens. Matter Mater. Phys.*, 1996, **54**, 1703–1710.
28 C. Hartwigsen, S. Goedecker and J. Hutter, *Phys. Rev. B: Condens. Matter Mater. Phys.*, 1998, **58**, 3641–3662.
29 M. Krack, *Theor. Chem. Acc.*, 2005, **114**, 145–152.
30 Y. Shao, *et al.*, *Mol. Phys.*, 2014, **113**, 184–215.
31 M. Bonomi, D. Branduardi, G. Bussi, C. Camilloni, D. Provasi, P. Raiteri, D. Donadio, F. Marinelli, F. Pietrucci, R. A. Broglia and M. Parrinello, *Comput. Phys. Commun.*, 2009, **180**, 1961–1972.
32 G. A. Tribello, M. Bonomi, D. Branduardi, C. Camilloni and G. Bussi, *Comput. Phys. Commun.*, 2014, **185**, 604–613.
33 S. B. Rempe and H. Jónsson, *Chem. Educ.*, 1998, **3**, 1–17.
34 P. Raiteri, A. Laio, F. L. Gervasio, C. Micheletti and M. Parrinello, *J. Phys. Chem. B*, 2006, **110**, 3533–3539.
35 A. Barducci, G. Bussi and M. Parrinello, *Phys. Rev. Lett.*, 2008, **100**, 020603.
36 C. Priest, M. R. VanGordon, C. S. Rempe, M. I. Chaudhari, M. J. Stevens, S. Rick and S. B. Rempe, in *Computing Potential of the Mean Force Profiles for Ion Permeation Through Channelrhodopsin Chimera, C1C2*, ed. R. E. Dempski, Springer US, New York, NY, 2021, pp. 17–28.
37 L. A. Prignano, M. J. Stevens, J. M. Vanegas, S. B. Rempe and R. E. Dempski, *PLoS One*, 2024, **19**, e0309553.
38 B. Poudel, R. T. Rajitha and J. M. Vanegas, *Nat. Commun.*, 2023, **14**, 4690.
39 J. D. Hunter, *Comput. Sci. Eng.*, 2007, **9**, 90–95.
40 J. C. B. Dietschreit, D. J. Diestler, A. Hulm, C. Ochsenfeld and R. Gómez-Bombarelli, *J. Chem. Phys.*, 2022, **157**, 084113.
41 J. Vanegas and M. Arroyo, *PLoS One*, 2014, **9**(12), 1–22.
42 E. Evans, *Annu. Rev. Biophys. Biomol. Struct.*, 2001, **30**, 105–128.

